Solar Cells, 16 (1986) 611 - 630

THEORY OF HIGH EFFICIENCY (Cd,Zn)S/$CuInSe_2$ THIN FILM SOLAR CELLS

CHANDRA GORADIA and MANJU GHALLA-GORADIA
Cleveland State University, Cleveland, OH 44115 (U.S.A.)

(Received July 15, 1985; accepted August 7, 1985)

Summary

A theoretical model is presented which allows the fitting of calculated results to both dark and illuminated current *versus* voltage characteristics at several temperatures above 300 K for two relatively high efficiency Boeing (Cd,Zn)S/$CuInSe_2$ thin film solar cells. The model is based on the assumptions that (1) the device is an n-(Cd,Zn)S/p-$CuInSe_2$ heterojunction, (2) interface recombination is the dominant loss current mechanism both in the dark and under illumination and (3) the interface recombination centers are negatively charged and their density increases under illumination. The model naturally explains the large A factors observed (about 1.4 - 2.2), the temperature dependence of the current–voltage characteristics, the non-translation between the illuminated and dark current–voltage characteristics and the observed low open-circuit voltages. In addition, results of parametric variation studies are presented which show that a maximum open-circuit voltage of about 550 mV is possible in these devices if the effective dopings in the selenide and sulfide are greater than 5×10^{15} cm^{-3} and greater than 5×10^{16} cm^{-3} respectively, while the negatively charged interface recombination level density is below 6×10^{10} cm^{-2}.

1. Introduction

The mechanisms of loss current in the n-(Cd,Zn)S/p-$CuInSe_2$ polycrystalline thin film solar cell in the dark and under illumination are not well understood. Not fully explained are (1) the large diode ideality or A factors (from 1.4 to larger than 2), (2) the temperature variation of the current density–voltage J–V characteristics, (3) the non-translation between the illuminated and dark J–V characteristics and (4) the low open-circuit voltages V_{oc}.

Several models have been proposed in an effort to explain the behavior of these solar cells. Rothwarf [1] and Eron and Rothwarf [2, 3] propose interface recombination as the dominant forward current mechanism, and they explain the large A factors under illumination and the non-translation

0379-6787/86/$3.50 © Elsevier Sequoia/Printed in The Netherlands

between illuminated and dark J-V curves entirely on the basis of interface charging and a voltage-dependent light-generated current. Potter and Sites [4] have done detailed measurements on light-induced shifts in the current-voltage I-V curves and attribute such shifts (non-translation) to the charging of interfacial states under illumination. Miller and Olsen [5] propose the loss current mechanism to be a combination of interface recombination and tunneling and explain the non-translation between light and dark J-V curves strictly on the basis of a light-induced increase in the pre-exponential current density factor J_0. Böer's model [6] is based on numerical integration of the two continuity equations and Poisson's equation and explains non-translation as due to the out-diffusion of photogenerated electrons from the narrow region near the interface, where most of the incoming photons are assumed to be absorbed, into the darker regions of the $CuInSe_2$.

While each of these previous models addresses one particular aspect of the problem, no model has, to our knowledge, theoretically fit both the dark and illuminated J-V characteristics at various temperatures. In this article, we present a model which allows us to do that. Our model is restricted to the relatively high efficiency (above 7.5%, AM 1, 300 K) Boeing (Cd,Zn)S/$CuInSe_2$ devices whose A factors show little or no dependence on temperature. (With minor changes in the electron affinity and band gap values of the sulfide layer, our model should most probably also apply to the relatively high efficiency $CdS/CuInSe_2$ devices.) In addition, our model is also restricted to temperatures above about 293 K. (It is suspected that at temperatures below 293 K the metal contact to the $CuInSe_2$ starts to become an injecting contact [7]. There is evidence of soft rectifier characteristics in such contacts below room temperature [8].) A different model may apply, most likely one that includes thermally assisted and/or pure tunneling, to the relatively low efficiency cells at normal operating temperatures and to the high efficiency cells at lower temperatures.

Our model assumes, as do all existing models, that the $CdS/CuInSe_2$ or (Cd,Zn)S/$CuInSe_2$ thin film solar cell is a true n-p heterojunction. However, recent electron-beam-induced current (EBIC) measurements [9] suggest that this device is a buried homojunction at a depth of about 0.7 μm from the sulfide-selenide interface. Even so, it may be possible to reconcile the EBIC data with the device being a heterojunction [10]. Also, most other experimental observations on this device provide strong arguments in favor of the device being a heterojunction, as is shown in Section 2. In any event, pending conclusive results from further experiments, our heterojunction-based model appears to explain the device behavior very well.

2. Quantitative model

2.1. Assumptions

Our model is based on the following assumptions.

(1) The device is an n-p heterojunction with a thermal equilibrium band diagram as shown in Fig. 1. Many observations support the assumption

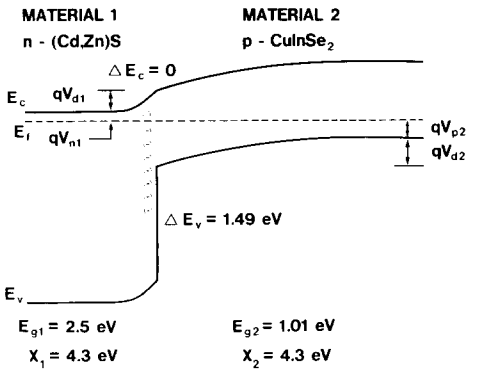

Fig. 1. Thermal equilibrium energy band diagram of an n-(Cd,Zn)S/p-$CuInSe_2$ heterojunction thin film solar cell. Actually, this is a scale drawing for dark cell BAC-845A with parameters as given in Tables 1 and 2 (see later).

that the device is a heterojunction. First, the near-ideal short-circuit current density, when taken in conjunction with an optical absorption depth in $CuInSe_2$ of about 0.1 μm and the long-term stability of this device, implies that the collection of photogenerated carriers occurs almost entirely in the high electric field space charge region of the $CuInSe_2$. The same implication results from the fact that the short-circuit current density does not degrade at all when this device is irradiated by 1 MeV electrons up to a fluence of 10^{16} electrons per square centimeter [11], since that means that J_{sc} is most probably immune to the degradation of diffusion length in the bulk of the $CuInSe_2$. Therefore, it appears that the space charge region in the $CuInSe_2$ extends at least over the first 0.1 μm or so in the $CuInSe_2$ from the heterojunction; it may, of course, extend to a greater depth in the $CuInSe_2$. This is a strong argument in favor of the heterojunction. Other arguments in favor of the heterojunction are also those that imply that the dominant loss current mechanism in the dark and under illumination is interface recombination. These are presented below in support of the second assumption.

(2) The forward current both in the dark and under illumination is primarily due to recombination at the hetero-interface. There is, however, a secondary contribution to the forward current from recombination in the $CuInSe_2$ space charge region. This assumption is based on several observations. First, a $J_0 \geqslant 10^{-7}$ A cm^{-2}, coupled with an A factor from about 1.4 to greater than 2, rules out bulk and external surface recombination current (also called diffusion current, as in crystalline homojunctions) as the primary forward current mechanism [12]. Secondly, the rather small activation energy for J_0 ($E_{a0} \leqslant 0.4$ eV in some cells [12]) rules out not only diffusion but also space charge recombination as primary current mechanisms, since the latter would require $E_{a0} = E_{g0}/2 > 0.5$ eV and the former would require $E_{a0} = E_{g0} > 1$ eV, where E_{g0} is the linearly extrapolated band gap of $CuInSe_2$ at 0 K. Thirdly, the essential temperature independence of the A factor or its mild increase with temperature, as occurs in the relatively high efficiency

cells to which this model is directed, implies that tunneling is not the dominant forward current mechanism. Finally, the remarkable resistance of this device to high fluences of 1 MeV electrons [11] and protons [13] implies that the recombination responsible for the forward current must occur in a rather narrow region of the cell, immune to degradation of diffusion length. The only likely very narrow region for a large amount of recombination to take place is the hetero-interface. Thus, it is our opinion that interface recombination is the most logical primary forward current mechanism. The need for space charge recombination as a secondary forward current mechanism will become clear later.

(3) The interface recombination centers are acceptor-like (*i.e.* neutral when unoccupied by an electron and negative when occupied), and the rate of interface recombination is limited by the availability of holes, *i.e.* of the electron and hole alternately trapped to complete a recombination event, the electron spends considerably more time trapped by an interface recombination center than does a hole. As a result, the recombination center is negatively charged most of the time. For simplicity, and to avoid an additional adjustable parameter, it is assumed that the interface recombination centers are always negatively charged, giving rise to an interface charge density $-qN_{ir}$ (C cm^{-2}) where N_{ir} (cm^{-2}) is the interface recombination level density and q is the magnitude of the electronic charge.

(4) Illumination of the device activates deep states at the interface and in the $CuInSe_2$ space charge region and thereby increases both components of the forward current density. The dependence on illumination level is non-linear, saturating at about 1 AM 1. These last two assumptions are consistent with the fact that the effective doping in the n-type sulfide is much greater than that in the p-type selenide, and with the non-translation between illuminated and dark J–V curves. They are also in common with the models of Potter and Sites [4] and Miller and Olsen [5].

2.2. Derivation

Applying standard theory to the heterojunction of Fig. 1 gives the total built-in band bending qV_d as

$$qV_d = \chi_2 - \chi_1 + E_{g2} - kT \ln\left(\frac{N_{c1}N_{v2}}{N_{d1}N_{a2}}\right) \tag{1}$$

Here, as throughout, subscripts 1 and 2 refer to the sulfide window and the selenide absorber respectively. Also, χ, E_g, N_c, N_v, N_d and N_a are respectively the electron affinity, the band gap, the effective densities of states in the conduction and valence bands and the effective donor and acceptor concentrations (majority carrier concentrations); V_d is the built-in voltage or diffusion potential, k is the Boltzmann constant and T is the absolute temperature.

Solving Poisson's equation in the two materials, under the depletion approximation, gives the individual built-in voltages V_{d1} and V_{d2} as

$$V_{d1} = \frac{qN_{d1}x_{n10}^2}{2\epsilon_{r1}\epsilon_0} \tag{2a}$$

$$V_{d2} = \frac{qN_{a2}x_{p20}^2}{2\epsilon_{r2}\epsilon_0} \tag{2b}$$

Here, x_{n10} and x_{p20} are the thermal equilibrium widths of the space charge regions, ϵ_r is the d.c. or low frequency relative permittivity (dielectric constant) and ϵ_0 is the permittivity of free space.

In non-equilibrium, the assumption of quasi-equilibrium gives the net voltages $V_{d1} - V_{j1}$ and $V_{d2} - V_{j2}$ as

$$V_{d1} - V_{j1} = \frac{qN_{d1}x_{n1}^2}{2\epsilon_{r1}\epsilon_0} \tag{3a}$$

$$V_{d2} - V_{j2} = \frac{qN_{a2}x_{p2}^2}{2\epsilon_{r2}\epsilon_0} \tag{3b}$$

Here, V_{j1} and V_{j2} are the components of the externally applied voltage appearing across the respective junction space charge regions. The non-equilibrium space charge region widths x_{p2} and x_{n1} are given by

$$x_{p2} = \frac{-\alpha_2 + (\alpha_2^2 - 4\alpha_1\alpha_3)^{1/2}}{2\alpha_1} \tag{4a}$$

$$x_{n1} = \frac{N_{a2}}{N_{d1}}x_{p2} + \frac{N_{ir}}{N_{d1}} \tag{4b}$$

where

$$\alpha_1 = \frac{qN_{a2}}{2\epsilon_{r2}\epsilon_0}\left(1 + \frac{N_{a2}\epsilon_{r2}}{N_{d1}\epsilon_{r1}}\right) \tag{5a}$$

$$\alpha_2 = \frac{qN_{a2}N_{ir}}{\epsilon_{r1}\epsilon_0 N_{d1}} \tag{5b}$$

$$\alpha_3 = \frac{qN_{ir}^2}{2\epsilon_{r1}\epsilon_0 N_{d1}} - (V_d - V_j) \tag{5c}$$

and

$$V_d = V_{d1} + V_{d2} \tag{6a}$$

$$V_j = V_{j1} + V_{j2} \tag{6b}$$

Equation (4b) represents Gauss' law, *i.e.* the net charge contained in the space charge regions and at the interface ($-qN_{ir}$ (C cm^{-2})) adds up to zero. When that is used in conjunction with the sum of eqns. (3a) and (3b), eqn. (4a) results, provided that α_1, α_2 and α_3 are defined by eqns. (5a) - (5c) and V_d and V_j by eqns. (6a) and (6b). From eqns. (4a) and (4b), the thermal equilibrium values x_{p20} and x_{n10} are obtained by setting $V_j = 0$ in eqn. (5c).

Next, following Rothwarf [1], the interface recombination current density is given by

$$J_{ir}(V_j) = qS_{ip}\Delta p_i(V_j)$$
$$= q\sigma_{ip}v_{th}N_{ir}\Delta p_i(V_j) \tag{7}$$

where the hole recombination velocity S_{ip} at the interface has been expressed as the product of the hole capture cross-section σ_{ip}, its thermal velocity v_{th} and the interface recombination level density N_{ir}. The excess hole concentration $\Delta p_i(V_j)$ at the interface is given by

$$\Delta p_i(V_j) = N_{v2}\exp\left\{-\frac{(V_{p2}+V_{d2})}{V_T}\right\}\left\{\exp\left(\frac{V_{j2}}{V_T}\right)-1\right\}$$
$$= N_{a2}\exp\left(-\frac{V_{d2}}{V_T}\right)\left\{\exp\left(\frac{V_j}{A_{ir}V_T}\right)-1\right\} \tag{8}$$

where $V_T = kT/q$ is the thermal voltage, $V_{p2} = (E_f - E_v)/q = V_T \ln(N_{v2}/N_{a2})$ and

$$A_{ir} \equiv \frac{V_j}{V_{j2}}$$
$$= 1 + \frac{V_{j1}}{V_{j2}} \tag{9}$$

is the diode ideality factor for interface recombination. Combining eqns. (7) and (8) we have

$$J_{ir} = q\sigma_{ip}v_{th}N_{ir}N_{a2}\exp\left(-\frac{V_{d2}}{V_T}\right)\left\{\exp\left(\frac{V_j}{A_{ir}V_T}\right)-1\right\} \tag{10a}$$

which, when expressed as

$$J_{ir} = J_{0ir}\left\{\exp\left(\frac{V_j}{A_{ir}V_T}\right)-1\right\} \tag{10b}$$

with

$$J_{0ir} = J_{00ir}\exp\left(-\frac{E_{a0}}{kT}\right) \tag{11}$$

gives

$$J_{0ir} = q\sigma_{ip}v_{th}N_{ir}N_{a2}\exp\left(-\frac{V_{d2}}{V_T}\right) \tag{12}$$

$$J_{00ir} = q\sigma_{ip}v_{th}N_{ir}N_{a2}\exp\left(\frac{q\beta}{k}\right) \tag{13}$$

and

$$E_{a0} = qV_{d20} \tag{14}$$

The factor $\exp(q\beta/k)$ in eqn. (13) is due to the linear temperature dependence of V_{d2}, namely

$$V_{d2}(T) = V_{d20} - \beta T \tag{15}$$

where V_{d20} is the linearly extrapolated value of V_{d2} at 0 K. The value of β can vary significantly among different cells. For one of the Boeing cells considered in this paper (BAC-845A) $\beta = |dV_{d2}/dT|$ was calculated to be approximately $10^{-3}\,\mathrm{V\,K^{-1}}$, giving $\exp(q\beta/k) \approx 10^5$ and $J_{00\,ir} \approx 10^4\,\mathrm{A\,cm^{-2}}$, as measured by Miller and Olsen [5]. It should be noted that eqn. (14) gives the activation energy for J_{0ir} to be qV_{d20}, the extrapolated (to 0 K) built-in band bending in the $CuInSe_2$, whose value may range from about 0.3 eV to more than 0.80 eV among different devices.

The A factor A_{ir} of eqn. (9) can be derived (see Appendix A) in terms of the fundamental parameters to give

$$A_{ir}(V_j) = 1 + \frac{N_{a2}\epsilon_{r2}}{N_{d1}\epsilon_{r1}} + \frac{2\epsilon_{r2}N_{ir}}{\epsilon_{r1}N_{d1}\{x_{p20} + x_{p2}(V_j)\}} \tag{16}$$

A_{ir} is a very mildly varying function of V_j as a result of $x_{p2}(V_j)$ in the last term in eqn. (16). It should be noted that A_{ir} is always greater than unity and, as will be shown later, can be greater than two, depending on the values of N_{a2}, N_{d1} and N_{ir}.

Finally, assuming that space charge recombination will occur entirely in the $CuInSe_2$ space charge region [14], since the J_0 for space charge recombination is proportional to the intrinsic carrier concentration n_i, which is negligible in the wide band gap window material, we can write the standard expression for the corresponding current density J_{scr} as

$$J_{scr} = J_{0scr}\left\{\exp\left(\frac{V_{j2}}{2V_T}\right) - 1\right\}$$

$$= J_{0scr}\left\{\exp\left(\frac{V_j}{2A_{ir}V_T}\right) - 1\right\} \tag{17}$$

with

$$J_{0scr} = \frac{qn_{i2}x_{p2}}{2\tau_{02}} \tag{18}$$

Here, n_{i2} is the intrinsic carrier concentration and τ_{02} is the effective recombination lifetime in the $CuInSe_2$ space charge region. It should be noted that the effective A factor for J_{scr} is $2A_{ir}$ because of the identity $V_{j2} = V_j/A_{ir}$ given by eqn. (9). It should also be noted that n_{i2} in eqn. (18) gives the activation energy for J_{0scr} to be $E_{g20}/2$ where E_{g20} is the band gap of $CuInSe_2$ extrapolated to 0 K.

The complete illuminated forward junction current density–voltage J_j–V_j characteristic, unaffected by series and shunt resistances, is given by

$$J_j = J_{0ir}\left\{\exp\left(\frac{V_j}{A_{ir}V_T}\right) - 1\right\} + J_{0scr}\left\{\exp\left(\frac{V_j}{2A_{ir}V_T}\right) - 1\right\} - J_{ph}(V_j) \tag{19}$$

where $J_{ph}(V_j)$ is the photogenerated current density, which may be somewhat dependent on the junction voltage through the voltage dependence of the space charge region width. The sum of the first two terms on the right-hand side of eqn. (19) is the forward diode current density in the dark and the loss current density J_{loss} under illumination. Since J_{0ir}, J_{0scr} and A_{ir} may be different under illumination than in the dark, in general, the dark forward and loss current densities at a given voltage V_j are not the same, leading to non-translation between illuminated and dark J_j-V_j curves. A voltage-dependent J_{ph} can also give rise to non-translation.

3. Calculated results

In this section we show the results of our attempt to fit the calculated dark and illuminated J_j-V_j curves at several temperatures to the corresponding measured curves for two Boeing n-(Cd,Zn)S/p-$CuInSe_2$ thin film solar cells, namely BAC-1038A and BAC-845A, for which detailed measurements are available. The measured data were provided by Miller and Olsen [7] in both their as-measured J-V form and in the J_j-V_j form, with the effects of series and shunt resistances removed. We shall use only the J_j-V_j data.

Figures 2 and 3 give the dark and illuminated J-V characteristics of the two cells on a linear scale at 303 K. Also given are values of some other pertinent parameters. Neither cell had an antireflection coating. It should be noted that BAC-845A had a higher V_{oc} and a higher efficiency in spite of a significantly larger amount of non-translation.

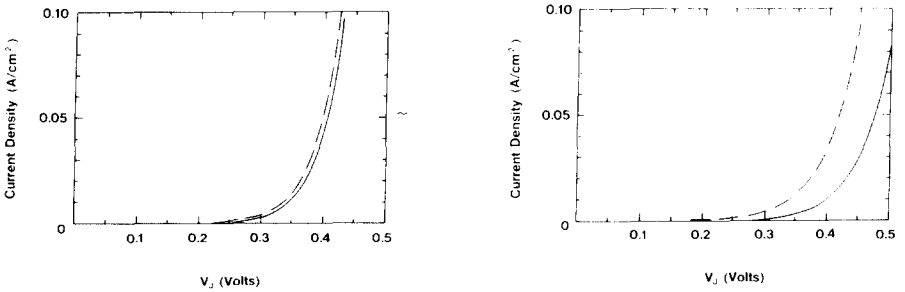

Fig. 2. Dark and illuminated (shifted by J_{sc}) current density *vs.* voltage characteristics at 303 K for cell BAC-1038A (dark, $J_0 = 0.61\ \mu A\ cm^{-2}$, $A = 1.38$; at about AM 1, $J_0 = 1.7\ \mu A\ cm^{-2}$, $A = 1.48$, $J_{sc} = 32\ mA\ cm^{-2}$, $V_{oc} = 380\ mV$): ——, J_j; - - -, $J_j + J_{sc}$.

Fig. 3. Dark and illuminated (shifted by J_{sc}) current density *vs.* voltage characteristics at 303 K for cell BAC-845A (dark, $J_0 = 1.2\ \mu A\ cm^{-2}$, $A = 1.71$; at about AM 1, $J_0 = 5\ \mu A\ cm^{-2}$, $A = 1.71$, $J_{sc} = 35\ mA\ cm^{-2}$, $V_{oc} = 390\ mV$): ——, J_j; - - -, $J_j + J_{sc}$. (The larger non-translation in this cell than in BAC-1038A should be noted. However, this cell has a slightly larger open-circuit voltage V_{oc}.)

3.1. Method of generating calculated J_j-V_j characteristics

Table 1 lists the values of the fixed parameters used in all calculations. We have assumed that the electron affinities χ_1 and χ_2 of the (Cd,Zn)S and $CuInSe_2$ are equal (each 4.3 eV). However, calculations will be shown later about the effect of varying χ_1 on the V_{oc} of the cell. The accurate value of E_{g1} is not critical to the calculations.

We have developed a computer code which calculates $J_j(V_j)$, using eqn. (19), at a large number of V_j values. The V_j increments get smaller on the steeper portion of the curve. In our model, the only cause of the voltage dependence of J_{ph} is the voltage dependence of the space charge width x_{p2} in the $CuInSe_2$. Detailed computer calculations showed the voltage dependence of J_{ph} to be slight; further, such dependence is fully accounted for by letting the shunt resistance R_{sh} have a different value under illumination than in the dark. Hence, in generating the illuminated J_j-V_j characteristic using eqn. (19), we used a fixed J_{ph} equal to the measured J_{sc} of the cell being fitted.

Starting with an assumed fixed effective doping $N_{a2} = 1 \times 10^{15}$ cm^{-3} in the $CuInSe_2$ [15], we varied N_{d1}, N_{ir} and τ_{02} until the calculated dark $\log_{10}(J_j)$ *versus* V_j plot gave a good fit to the measured plot at a single temperature $T = 303$ K. Next, all parameters were kept constant, and only the temperature was varied to generate the calculated plots at the other temperatures. No fitting was attempted at the other temperatures. For the illuminated plots, only N_{ir} and τ_{02} were allowed to vary until a good fit at 303 K was obtained. Again, only the temperature was varied to obtain curves at other temperatures.

The three adjustable or fitting parameters, N_{d1}, N_{ir} and τ_{02}, were found to be both necessary and sufficient to obtain good fits with measured data.

TABLE 1

General parameter values

Parameter	*Value*
Electron affinity $\chi_1 = \chi_2$	4.3 eV
Low frequency dielectric constant	
ϵ_{r1}	10.0
ϵ_{r2}	13.6
Band gap at 300 K	
E_{g1}	2.5 eV
E_{g2}	1.01 eV
Temperature coefficient dE_{g2}/dT of band gap	-3.1×10^{-4} eV K^{-1}
Intrinsic carrier concentration n_{i2} at 300 K	2.31×10^{10} cm^{-3}
Effective density of states	
N_{c1}	2×10^{18} cm^{-3}
N_{v2}	1×10^{19} cm^{-3}

Subscripts 1 and 2 are for (Cd,Zn)S and $CuInSe_2$ respectively.

The J_j-V_j curves were sensitive to τ_{02} values only at the lower voltages, while the entire curves were rather sensitive to N_{d1} and N_{ir} over certain ranges of these parameters.

3.2. Comparison between calculated and measured results

Figures 4 and 5 show the dark and illuminated J_j-V_j curves of cells BAC-1038A and BAC-845A respectively at several temperatures. The full curves in these figures are our calculated curves; the points are the measured values supplied by Miller and Olsen [7]. It is seen that, in most cases, the fit between calculated and measured curves is excellent. The reason for the somewhat poor fits for the dark BAC-845A at the higher temperatures is not clear. As for the poor fits below 300 K, it appears that more recombination is taking place in the cell than accounted for by our model; the fact that, in most cases, the mismatch is greater at the lower voltages indicates that hole

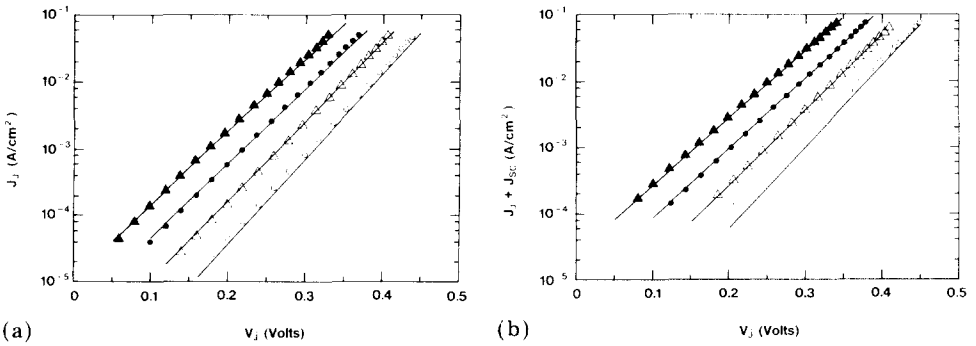

Fig. 4. (a) Dark and (b) illuminated $\log_{10}(J_j)$-V_j curves for cell BAC-1038A at several temperatures: ▲ (343 K), ● (323 K), △ (303 K), ○ (283 K), measured values supplied by Miller and Olsen [7]; ——, calculated values using our model.

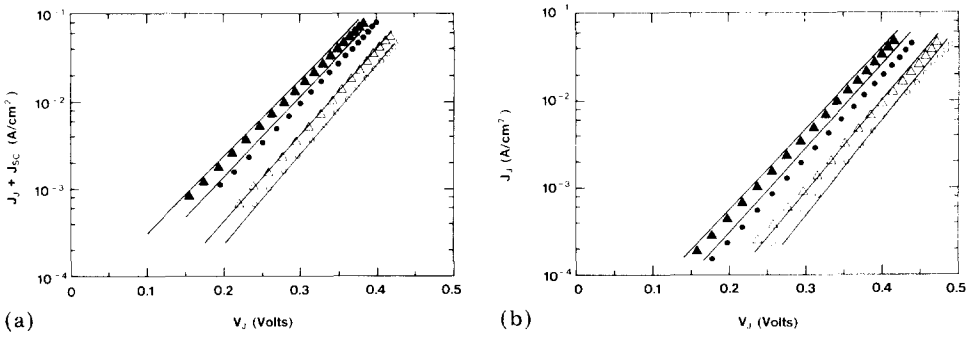

Fig. 5. (a) Dark and (b) illuminated $\log_{10}(J_j)$-V_j curves for cell BAC-845A at several temperatures: ▲ (333 K), ● (323 K), △ (303 K), ○ (293 K), measured values supplied by Miller and Olsen [7]; ——, calculated values using our model.

injection from the back contact into the $CuInSe_2$ could be a possible cause of the mismatch.

In principle, almost all relevant aspects of the behavior of these two Boeing cells are explained quite naturally by our model in the process of fitting the calculated to the measured J_j-V_j curves at several temperatures. However, more detailed discussion is needed to understand fully the behavior of these cells. This is provided in Section 4.

4. Discussion of calculated results

Figure 6 shows $J_{ir}(V_j)$, $J_{scr}(V_j)$ and their sum $J_{loss}(V_j)$ for the illuminated cell BAC-845A at 303 K. It is seen that, although J_{ir} is the dominant loss current component, with $J_{0ir} = 1.49 \times 10^{-6}$ A cm^{-2} and $A_{ir} = 1.5$, while J_{scr} is considerably smaller, with $J_{0scr} = 11 \times 10^{-6}$ A cm^{-2} and $A_{scr} = 2A_{ir} = 3.0$, their sum J_{loss} has an overall $J_0 = 6.8 \times 10^{-6}$ A cm^{-2} and $A = 1.76$. Thus, the relative values of the different quantities are such that the sum of two exponentials behaves like a third exponential with overall J_0 and A values somewhere between those of the individual curves.

Although V_{oc} appears to be determined very much by J_{ir} alone, J_{scr} plays a role at the lower voltages and in determining the overall J_0 and A factor. Essentially the same V_{oc} is obtained from $V_{oc} = A_{ir}V_T \ln(J_{sc}/J_{0ir})$ as from $V_{oc} = AV_T \ln(J_{sc}/J_0)$. The above behavior is common to the dark and illuminated curves of both cells. Thus, space charge recombination does not seem to have real significance in these cells, except for reducing the fill factor somewhat as a result of the slightly higher J_{loss} at maximum power. This point will become strikingly evident later (Fig. 9).

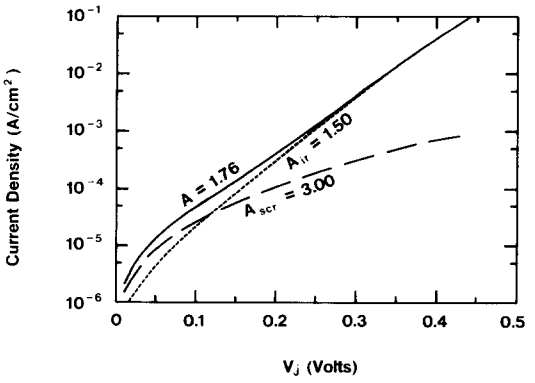

Fig. 6. Illuminated current density *vs.* voltage characteristics for cell BAC-845A, illustrating the need for space charge recombination as a secondary loss current mechanism to allow fitting the calculated to measured J_j-V_j curves at the lower voltages. Although V_{oc} is determined almost entirely by interface recombination, the overall measured J_0 and A factor are controlled very significantly by space charge recombination: ——, J_{loss}; ----, J_{ir}; – – –, J_{scr}.

TABLE 2

Fitting and internal parameter values for cells BAC-1038A and BAC-845A at 303 K

	N_{d1} (cm^{-3})	N_{ir} (cm^{-2})	τ_{02} (ns)	A_{ir}[a]	A[a]	J_0 ($\mu A\,cm^{-2}$)	J_{0ir} ($\mu A\,cm^{-2}$)	J_{0scr} ($\mu A\,cm^{-2}$)	x_{p20} (μm)	x_{n10} (μm)	V_{d2} (mV)	V_{d1} (mV)
BAC-1038A												
Dark	1.51×10^{16}	1.41×10^{11}	190	1.33	1.50	1.40	0.39	0.89	0.741	0.142	364	277
Illuminated	1.51×10^{16}	1.45×10^{11}	40	1.34	1.54	2.40	0.56	4.20	0.732	0.145	356	285
BAC-845A												
Dark	8.1×10^{15}	7.70×10^{10}	55	1.40	1.56	0.57	0.18	3.10	0.745	0.187	369	256
Illuminated	8.1×10^{15}	9.60×10^{10}	15	1.50	1.76	6.80	1.49	11.0	0.693	0.204	320	305

It is assumed that $\chi_1 = \chi_2 = 4.3$ eV, $N_{a2} = 1 \times 10^{15}$ cm^{-3} and $E_{g2} = 1.01$ eV.
[a] At $V_j \approx 400$ mV.

TABLE 3

Calculated values of A_{ir} and A at various temperatures for cell BAC-1038A

	$N_{a2}\epsilon_{r2}/N_{d1}\epsilon_{r1}$	*Calculated values of A_{ir} and A at the following temperatures*							
		283 K		*303 K*		*323 K*		*343 K*	
		A_{ir}	A	A_{ir}	A	A_{ir}	A	A_{ir}	A
Dark	0.09	1.30	1.39	1.32	1.42	1.33	1.46	1.35	1.53
Illuminated	0.09	1.31	1.43	1.33	1.46	1.34	1.50	1.36	1.58

Table 2 lists the values of the adjustable parameters N_{d1}, N_{ir} and τ_{02} needed to obtain good fits to the dark and illuminated measured curves of these cells at 303 K. Also given are the values of the interface recombination A factor A_{ir}, the overall effective A factor, the pre-exponential current density factors J_0, J_{0ir} and J_{0scr}, the thermal equilibrium space charge widths x_{p20} and x_{n10} and the built-in voltages V_{d2} and V_{d1}. The values of A_{ir}, A and the overall effective J_0 are given for $V_j = 400$ mV, a value near V_{oc}, rather than based on the least-squares straight lines covering the entire voltage ranges of the measured plots, as done by Miller and coworkers [5, 12]. Hence, our values of J_0 and A differ slightly from theirs.

Tables 3 and 4 give the calculated values of A_{ir} and the overall A at various temperatures for cells BAC-1038A and BAC-845A respectively. These are at $V_j = 350$ mV because some of the higher temperature curves do not extend to $V_j = 400$ mV. Also given are values of $N_{a2}\epsilon_{r2}/N_{d1}\epsilon_{r1}$, the second term on the right-hand side in eqn. (16), which sets the lower limit on the A factor. The difference between A_{ir} and $1 + N_{a2}\epsilon_{r2}/N_{d1}\epsilon_{r1}$ gives the contribution to A_{ir} from the third (interface recombination level density) term in eqn. (16).

On the basis of Figs. 4 - 6 and Tables 2 - 4, we may note the following points.

(1) The values of N_{d1}, N_{ir} and τ_{02} in Table 2 needed to fit the measured curves of Figs. 4 and 5 are quite reasonable; N_{d1} is generally believed to be 10 - 15 times N_{a2}, N_{ir} is about the same as independently inferred by Potter and Sites [4, 16] and τ_{02} values are also of the right order of magnitude. Since the curves are not very sensitive to τ_{02}, these values may be somewhat crude.

(2) The values of x_{p20} in Table 2 agree well with those obtained from capacitance–voltage measurements on some other Boeing cells by Sites [17] and by Miller [15], corresponding to a zero-bias capacitance of about 15 nF cm^{-2}. Also, the V_{d20} values obtained from the dark and illuminated V_{d2} values compare well with the corresponding measured activation energies for J_0 for cell BAC-845A [5].

TABLE 4

Calculated values of A_{ir} and A at various temperatures for cell BAC-845A

	$N_{a2}\epsilon_{r2}/N_{d1}\epsilon_{r1}$	*Calculated values of A_{ir} and A at the following temperatures*							
		293 K		*303 K*		*323 K*		*333 K*	
		A_{ir}	A	A_{ir}	A	A_{ir}	A	A_{ir}	A
Dark	0.168	1.38	1.54	1.39	1.54	1.40	1.57	1.41	1.58
Illuminated	0.168	1.47	1.64	1.48	1.66	1.50	1.73	1.51	1.77

(3) It is seen from Table 2 that illumination causes a small increase in N_{ir} and a substantial reduction in τ_{02}. The N_{ir} increase leads to an increase in x_{n10} and V_{d1} at the expense of x_{p20} and V_{d2}, and a corresponding increase in J_{0ir} and A_{ir} (also A_{scr}). The τ_{02} reduction increases J_{0scr}. Overall, both J_0 and A are increased. It is this increase in J_0 and A under illumination which is the primary cause of non-translation in these devices. The smaller increase in J_0 and A under illumination for cell BAC-1038A, leading to a smaller non-translation than for cell BAC-845A, should be noted. A small additional contribution to non-translation comes from the voltage dependence of J_{ph} which, in our model, is accounted for by a reduced R_{sh} under illumination.

(4) For these high efficiency solar cells, Tables 3 and 4 show that the A factor increases mildly with increasing temperature. If tunneling were the dominant loss current mechanism, then the A factor should decrease with increasing temperature such that $1/AkT$ would remain constant. Therefore, at least in these cells, tunneling does not play an important role as a loss current mechanism. Miller and Olsen arrived at the same conclusion for cell BAC-845A [5, 15].

5. Explanation of observed behavior

We now explain the observed behavior of these cells, namely the large A factors and their temperature dependence, the non-translation between illuminated and dark J_j-V_j curves and, finally, the low V_{oc} values.

5.1. Large A factors

According to eqn. (16), our model predicts A_{ir} to be always larger than unity. The lower limit on A_{ir} is $1 + N_{a2}\epsilon_{r2}/N_{d1}\epsilon_{r1}$ which is the same as the total A factor originally predicted by Rothwarf [1]. However, the last term in eqn. (16) may add significantly to A_{ir}, *e.g.* 0.25 for BAC-1038A and 0.33 for BAC-845A under illumination. In addition, space charge recombination, which has no effect on V_{oc}, further substantially increases the overall observed A factor, *e.g.* by 0.20 for BAC-1038A and 0.26 for BAC-845A under illumination. For cells with smaller N_{d1}/N_{a2} ratios or larger values of N_{ir} or larger contribution from space charge recombination, A factors as large as 2 or even higher are naturally explained by our model.

5.2. Temperature dependence of J_j-V_j and A

The temperature dependence of J_0 and the A factors, obtained from J_j-V_j curves at several temperatures, is commonly used as a diagnostic tool to identify the loss current mechanism in a solar cell [12]. For the five commonly encountered loss current mechanisms, standard theory predicts the following: (1) thermionic emission (activation energy E_{a0} for J_0 of $q\phi_{B0}$, the barrier height at 0 K, $A = 1$, independent of T); (2) bulk and surface recombination (diffusion) ($E_{a0} = E_{g0}$, $A = 1$, independent of T); (3) space charge recombination ($E_{a0} = E_{g0}/2$, $A = 2$, independent of T);

(4) interface recombination ($E_{a0} = qV_{d20}$, $A > 1$, A mildly increases with increasing T); (5) tunneling ($E_{a0} < qV_{d0}$ and $A \propto 1/T$ so that $B = 1/AkT$ is constant). Of course, in real devices, more than one mechanism may operate simultaneously, dominating over different voltage ranges.

In our particular case, calculations show that x_{p20} and $x_{p2}(V_j)$ in the last term of eqn. (16) decrease mildly with increasing temperature. This causes A_{ir} to increase mildly with increasing temperature. However, since $A_{scr} = 2A_{ir}$, A_{scr} increases more rapidly with increasing temperature. The net effect of A_{ir} and A_{scr} is that the overall A factor increases with temperature as shown in Tables 3 and 4. It should be noted that, as would be expected, the increase in A with temperature is stronger for the illuminated than the dark case. This is because of the reduction in τ_{02} under illumination, making the space charge recombination contribution more significant. As pointed out earlier, tunneling does not play a significant role in these cells.

5.3. Non-translation

This point has been discussed in Section 4. Here, we would only like to add that our approach on this issue is the same as that of Miller and Olsen [5], and of Potter and Sites [4] but is very different from that of Eron and Rothwarf [2, 3] and of Boër [6].

5.4. Low V_{oc} values

In our model, the open-circuit voltage V_{oc} is given, to a very close approximation, by

$$V_{oc} = A_{ir}V_T \ln\left(\frac{J_{sc}}{J_{0ir}}\right) \tag{20}$$

Thus, in order to obtain a high V_{oc}, we need a low J_{0ir} and a large A_{ir}. However, J_{0ir} is proportional to both N_{ir} and N_{a2} while A_{ir} has terms which are individually proportional to N_{ir} and N_{a2}. Further, if J_{0ir} is reduced by increasing V_{d2}, then A_{ir} is reduced because of the increase in x_{p20} and x_{p2} with V_{d2}. Thus, it appears that J_{0ir} and A_{ir} are linked, both increasing or decreasing together. However, as will be shown in Section 6, it is possible, at least theoretically, to choose values of N_{a2}, N_{d1} and N_{ir}, and hence combinations of J_{0ir} and A_{ir}, which could give considerably higher V_{oc} values (up to 550 mV) than those measured in existing cells. The low V_{oc} values in existing cells are then explained on the basis of values of N_{a2}, N_{d1} and N_{ir} which always yield poor combinations of J_{0ir} and A_{ir}. We suspect that current fabrication methods link N_{a2}, N_{d1} and N_{ir} in such a way that desirable (relatively large) values of N_{a2} and N_{d1} also give undesirably large values of N_{ir}, yielding the low observed V_{oc} values.

As an example of the fact that it is the combination of J_{0ir} and A_{ir} which determines V_{oc}, not either parameter alone, it should be noted that BAC-845A has a slightly higher V_{oc} than BAC-1038A, in spite of having a J_{0ir} nearly three times larger. The higher A_{ir} of BAC-845A more than compensates for the higher J_{0ir}.

6. Design considerations for high V_{oc} values

We have performed detailed parametric variation calculations in an attempt to answer the following questions.

(1) How sensitive is V_{oc} to N_{ir}, for different combinations of N_{a2} and N_{d1}?

(2) Even if we are resigned to a high N_{ir} value of about 10^{11} cm^{-2}, can N_{a2} and N_{d1}, which presumably can be controlled (at least to a certain extent), be chosen to yield high V_{oc}?

(3) How does V_{oc} depend on other parameters such as τ_{02} and χ_1?

(4) What maximum V_{oc} can realistically be expected for this device?

These results will now be discussed.

6.1. V_{oc} dependence on N_{ir}

Figure 7 shows V_{oc} *versus* N_{ir} for several combinations of N_{a2} and N_{d1}. It is seen that, for $N_{ir} \geqslant 8 \times 10^{10}$ cm^{-2}, V_{oc} drops precipitously with increasing N_{ir}, and more strongly so for the lower values of N_{a2} and N_{d1}. It is then clear that the low V_{oc} values (370 - 430 mV) for existing cells are due to (a) low values of N_{a2} (5×10^{14} - 1×10^{15} cm^{-3}, as measured by Miller [15]), (b) relatively low N_{d1}/N_{a2} ratios (7.5 - 10 for some cells) and (c) high values of N_{ir} (8×10^{10} - 1.5×10^{11} cm^{-2}). Figure 7 also shows that V_{oc} values of 470 - 550 mV may be possible if $N_{a2} > 10^{15}$ cm^{-3} and $N_{d1} > 1.5 \times 10^{16}$ cm^{-3}.

6.2. V_{oc} dependence on N_{a2} and N_{d1}/N_{a2} ratio

Figures 8(a) and 8(b) show, for $N_{ir} = 1 \times 10^{11}$ cm^{-2} and $N_{ir} = 7.5 \times 10^{10}$ cm^{-2} respectively, plots of V_{oc} *versus* the N_{d1}/N_{a2} ratio for different values of N_{a2}. It is seen that for each N_{a2} and N_{ir} there is an optimum N_{d1}/N_{a2} ratio

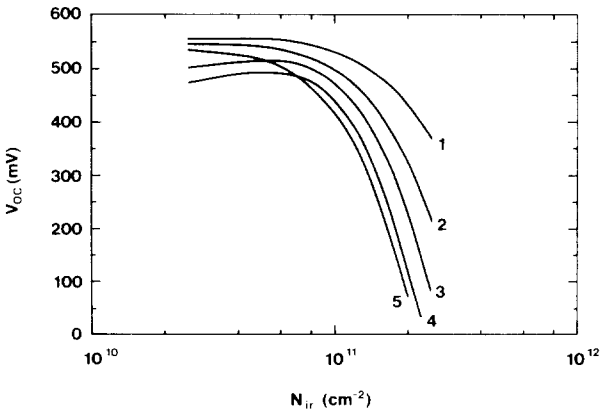

Fig. 7. Dependence of open-circuit voltage V_{oc} on negatively charged interface recombination level density N_{ir} for several combinations of effective dopings N_{a2} and N_{d1} ($T = 303$ K): curve 1, $N_{a2} = 5 \times 10^{15}$ cm^{-3}, $N_{d1} = 5 \times 10^{16}$ cm^{-3}; curve 2, $N_{a2} = 2.5 \times 10^{15}$ cm^{-3}, $N_{d1} = 2.5 \times 10^{16}$ cm^{-3}; curve 3, $N_{a2} = 1 \times 10^{15}$ cm^{-3}, $N_{d1} = 1.5 \times 10^{16}$ cm^{-3}; curve 4, $N_{a2} = 5 \times 10^{14}$ cm^{-3}, $N_{d1} = 1 \times 10^{16}$ cm^{-3}; curve 5, $N_{a2} = 1 \times 10^{15}$ cm^{-3}, $N_{d1} = 1 \times 10^{16}$ cm^{-3}.

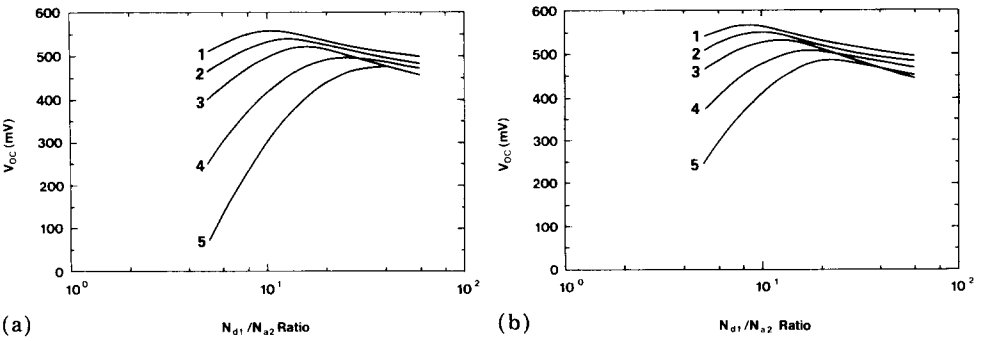

Fig. 8. Dependence of V_{oc} on effective doping ratio N_{d1}/N_{a2} for different N_{a2} ($T = 303$ K): curve 1, $N_{a2} = 1 \times 10^{16}$ cm^{-3}; curve 2, $N_{a2} = 5 \times 10^{15}$ cm^{-3}; curve 3, $N_{a2} = 2.5 \times 10^{15}$ cm^{-3}; curve 4, $N_{a2} = 1 \times 10^{15}$ cm^{-3}; curve 5, $N_{a2} = 5 \times 10^{14}$ cm^{-3}; (a) $N_{ir} = 10^{11}$ cm^{-2}; (b) $N_{ir} = 7.5 \times 10^{10}$ cm^{-2}.

which increases with decreasing N_{a2} and increasing N_{ir}. This type of behavior is due to the fact that a large N_{a2} and a large N_{d1}/N_{a2} ratio increase V_{d2} and reduce J_{0ir}, thereby increasing V_{oc}. However, after a certain point, further increases in the N_{d1}/N_{a2} ratio do not reduce J_{0ir} any further but reduce A_{ir}, reducing V_{oc}; hence there is an optimum ratio of N_{d1}/N_{a2}. Again, the low V_{oc} values are seen to be due to low N_{a2}, a low N_{d1}/N_{a2} ratio and high N_{ir}. As a direct evidence of the need for a high N_{d1}/N_{d2} ratio, it is to be noted that V_{oc} values of above 390 mV have been obtained with heavily indium-doped CdS window layers (instead of (Cd,Zn)S) and that, in a large batch of cells fabricated, both with and without an undoped CdS layer, the only ones with reasonably high V_{oc} values (above 370 mV) were those without the undoped CdS layer [18].

From a comparison of Figs. 8(a) and 8(b), it is seen that, while a lower N_{ir} of 7.5×10^{10} cm^{-2} does not increase the maximum achievable V_{oc} to any significant degree, it does substantially improve the V_{oc} values for low N_{d1}/N_{a2} ratios at low N_{a2} values compared with the higher N_{ir} (1×10^{11} cm^{-2}) case. Thus, it is very advantageous to reduce N_{ir} if that is somehow possible. It is also seen that, for high N_{d1}/N_{a2} ratios, V_{oc} is essentially the same for $N_{ir} = 7.5 \times 10^{10}$ cm^{-2} as it is for $N_{ir} = 10^{11}$ cm^{-2}. Since in our model, non-translation is mainly due to an increase in N_{ir} under illumination, this means that high N_{d1}/N_{a2} ratios reduce or eliminate non-translation. This has been observed by Birkmire *et al.* [19] who found that a rather heavily indium-doped CdS layer eliminated non-translation.

6.3. V_{oc} dependence on τ_{02}

Figure 9 shows the dependence, or rather the lack thereof, of V_{oc} on the effective recombination lifetime τ_{02} in the $CuInSe_2$ space charge region. This clearly shows that, even with τ_{02} as low as 10 ns, interface recombination is the dominant loss current mechanism at voltages in the vicinity of V_{oc}. However, at lower forward voltages, the space charge recombination

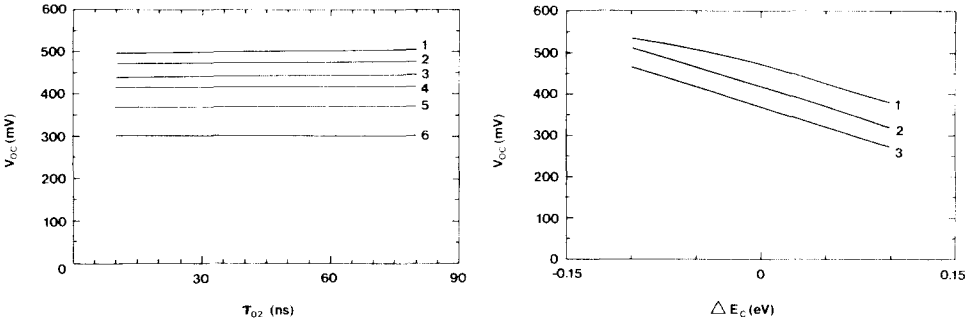

Fig. 9. Dependence of V_{oc} on the effective recombination lifetime τ_{02} in the space charge region of $CuInSe_2$ for different combinations of N_{a2}, N_{d1} and N_{ir}. Curve 5 closely approximates conditions for cell BAC-1038A ($T = 303$ K): curve 1, $N_{a2} = 2.5 \times 10^{15}$ cm^{-3}, $N_{d1} = 2.5 \times 10^{16}$ cm^{-3}, $N_{ir} = 1 \times 10^{11}$ cm^{-2}; curve 2, $N_{a2} = 1.0 \times 10^{15}$ cm^{-3}, $N_{d1} = 1.5 \times 10^{16}$ cm^{-3}, $N_{ir} = 1 \times 10^{11}$ cm^{-2}; curve 3, $N_{a2} = 5.0 \times 10^{14}$ cm^{-3}, $N_{d1} = 1.0 \times 10^{16}$ cm^{-3}, $N_{ir} = 1 \times 10^{11}$ cm^{-2}; curve 4, $N_{a2} = 1.0 \times 10^{15}$ cm^{-3}, $N_{d1} = 1.0 \times 10^{16}$ cm^{-3}, $N_{ir} = 1 \times 10^{11}$ cm^{-2}; curve 5, $N_{a2} = 1.0 \times 10^{15}$ cm^{-3}, $N_{d1} = 1.5 \times 10^{16}$ cm^{-3}, $N_{ir} = 1.5 \times 10^{11}$ cm^{-2}; curve 6, $N_{a2} = 5.0 \times 10^{14}$ cm^{-3}, $N_{d1} = 5.0 \times 10^{15}$ cm^{-3}, $N_{ir} = 1 \times 10^{11}$ cm^{-2}.

Fig. 10. Dependence of V_{oc} on conduction band edge discontinuity $\Delta E_c = \chi_1 - \chi_2$ with χ_2 fixed at 4.3 eV. Curve 3 approximates conditions for cell BAC-1038A ($T = 303$ K, $N_{a2} = 1 \times 10^{15}$ cm^{-3}): curve 1, $N_{ir} = 1 \times 10^{11}$ cm^{-2}, $N_{d1} = 1.5 \times 10^{16}$ cm^{-3}; curve 2, $N_{ir} = 1 \times 10^{11}$ cm^{-2}, $N_{d1} = 1 \times 10^{16}$ cm^{-3}; curve 3, $N_{ir} = 1.5 \times 10^{11}$ cm^{-2}, $N_{d1} = 1.5 \times 10^{16}$ cm^{-3}.

current contribution to the total loss current is non-negligible; its primary effect is to increase the overall effective A factor and to reduce the fill factor.

6.4. V_{oc} dependence on χ_1

Figure 10 shows plots of V_{oc} as a function of conduction band edge discontinuity $\Delta E_c = \chi_1 - \chi_2$ at the heterojunction interface, for several values of N_{d1} and N_{ir}, with $N_{a2} = 10^{15}$ cm^{-3}. The calculations were made with a fixed $\chi_2 = 4.3$ eV for the $CuInSe_2$, and χ_1 of the sulfide window was varied from 4.2 eV (negative ΔE_c) to 4.4 eV (positive ΔE_c). It was assumed that, for the negative ΔE_c values, a spike discontinuity of up to 0.1 eV height is transparent to conduction electrons, with no impedance to their flow. It is seen that a smaller ΔE_c (near-zero or negative) increases V_{oc}. This is because it increases V_d and therefore V_{d2}. This explains why, with all other parameters the same, a (Cd,Zn)S window (about 20% Zn) gives a higher V_{oc} than a CdS window. By the same token, increasing χ_2 of the absorber would also increase V_{oc} if it does not at the same time create some other complications.

7. Conclusions

In this article, using a quantitative model of the relatively high efficiency n-(Cd,Zn)S/p-$CuInSe_2$ polycrystalline thin film solar cell, we have shown

that it is possible to model this device in a satisfactory manner and to explain key aspects of its observed behavior, namely the large A factors, the temperature variation of the J_j-V_j characteristics, the non-translation between illuminated and dark J_j-V_j curves and its elimination by a large ratio of dopings in the sulfide and selenide and the low V_{oc} values in existing devices. In addition, with the help of a parametric variation study, we have identified the principal causes of low open-circuit voltages in existing devices to be low effective dopings in both the selenide and the sulfide layers and large values of the negatively charged interface recombination level density N_{ir}. Our calculations show that the open-circuit voltage V_{oc} is rather sensitive to the values of N_{a2}, the N_{d1}/N_{a2} ratio and especially to N_{ir}; proper combinations of these three parameters, if achievable in practice, could yield V_{oc} values as high as 550 mV. It is recommended that future research be directed at fabricating devices with high end values of effective dopings in the sulfide and selenide layers adjacent to the interface, perhaps with the help of some barrier material which prevents or reduces the interdiffusion of cadmium and copper between these layers. Any successful efforts at reducing the interface recombination density N_{ir}, perhaps by reducing the lattice mismatch between the two layers, would also be very rewarding.

Acknowledgments

Several individuals have contributed generously to this work. Dr. Wesley A. Miller and Dr. Larry C. Olsen of the Joint Center for Graduate Study supplied complete measured data on two Boeing cells. Dr. James R. Sites of Colorado State University provided some carefully measured capacitance data. Mr. Nasser Noori, Mr. Ramon Lopez and Mr. Ralph Clark, all of Cleveland State University, helped with the computer simulation and data reduction. Dr. Allen M. Hermann of the Solar Energy Research Institute provided helpful comments and encouragement. Our sincere thanks to all.

References

1 A. Rothwarf, *IEEE Trans. Electron Devices, 29* (10) (1982) 1513.
2 M. Eron and A. Rothwarf, *Appl. Phys. Lett., 44* (1) (1984) 131.
3 M. Eron and A. Rothwarf, *J. Appl. Phys., 57* (6) (1985) 2275.
4 R. R. Potter and J. R. Sites, *IEEE Trans. Electron Devices, 31* (5) (1984) 571.
5 W. A. Miller and L. C. Olsen, *IEEE Trans. Electron Devices, 31* (5) (1984) 654.
6 K. W. Böer, Annual Tech. Report on SERI Contract No. XL4-04040-1, April 1984 - March 1985, University of Delaware.
7 W. A. Miller, personal communication, 1984.
8 B. Tell and P. M. Bridenbaugh, *J. Appl. Phys., 48* (6) (1977) 2477.
9 R. Matson, D. Cahen, R. Ahrenkiel and R. Noufi, Tech. Digest of SERI Polycrystalline Thin Film Review Meet., Oct. 1984, Golden, CO, SERI/CP-211-2548, p. 117.
10 C. Goradia, to be published.
11 C. F. Gay, R. R. Potter, D. P. Tanner and B. E. Anspaugh, *Proc. 17th Photovoltaic Specialists' Conf., Orlando, FL, May 1984*, IEEE Publ. No. 84CH2019-8, p. 151.

12 L. C. Olsen, W. A. Miller and F. W. Addis, Tech. Digest of SERI Polycrystalline Thin Film Review Meet., May 1983, Golden, CO, SERI/CP-211-1985, p. 135.
13 H. Dursch, W. Chen and D. Russell, Space Photovoltaic Research and Technology Conf., CP-2408, NASA-Lewis Research Center, Cleveland, OH, May 1985, p. 165.
14 A. L. Fahrenbruch and R. H. Bube, *Fundamentals of Solar Cells*, Academic Press, New York, 1983, p. 148.
15 W. A. Miller, Current transport in (Cd,Zn)S/$CuInSe_2$ solar cells, *Ph.D. Thesis*, Washington State University, Richland, WA, 1984.
16 R. R. Potter, Light-induced band structure modifications in $CuInSe_2$ and related photovoltaic cells, *Ph.D. Thesis*, Colorado State University, Fort Collins, CO, 1983.
17 J. R. Sites, personal communication, 1984.
18 R. W. Birkmire, R. B. Hall, J. E. Phillips and J. D. Meakin, Final Tech. Report on SERI Contract No. XL-3-03065-01, March 1983 to March 1984, SERI/STR-211-2516.
19 R. W. Birkmire, R. B. Hall and J. E. Phillips, *Proc. 17th Photovoltaic Specialists' Conf., Orlando, FL, May 1984*, IEEE Publ. No. 84CH2019-8, p. 882.

Appendix A: Derivation of $A_{ir}(V_j)$ of equation (16)

Combination of eqns. (2a) and (3a) and eqns. (2b) and (3b) gives

$$V_{j1} = \frac{qN_{d1}}{2\epsilon_{r1}\epsilon_0}(x_{n10}^2 - x_{n1}^2) \tag{A1}$$

$$V_{j2} = \frac{qN_{a2}}{2\epsilon_{r2}\epsilon_0}(x_{p20}^2 - x_{p2}^2) \tag{A2}$$

Hence

$$\frac{V_{j1}}{V_{j2}} = \frac{N_{d1}\epsilon_{r2}}{N_{a2}\epsilon_{r1}} \frac{x_{n10}^2 - x_{n1}^2}{x_{p20}^2 - x_{p2}^2} \tag{A3}$$

Using eqn. (4b)

$$x_{n10}^2 - x_{n1}^2 = \frac{N_{a2}^2}{N_{d1}^2}(x_{p20}^2 - x_{p2}^2) + \frac{2N_{a2}N_{ir}}{N_{d1}^2}(x_{p20} - x_{p2}) \tag{A4}$$

Hence

$$\frac{V_{j1}}{V_{j2}} = \frac{N_{a2}\epsilon_{r2}}{N_{d1}\epsilon_{r1}} + \frac{2\epsilon_{r2}N_{ir}}{\epsilon_{r1}N_{d1}(x_{p20} + x_{p2})} \tag{A5}$$

giving

$$A_{ir} = \frac{V_j}{V_{j2}} = 1 + \frac{V_{j1}}{V_{j2}} = 1 + \frac{N_{a2}\epsilon_{r2}}{N_{d1}\epsilon_{r1}} + \frac{2\epsilon_{r2}N_{ir}}{\epsilon_{r1}N_{d1}\{x_{p20} + x_{p2}(V_j)\}} \tag{A6}$$